Significance of tensor coupling effect on shell evolutions and relativistic symmetries in calcium isotopes*

Xin-Xing Shi (史新星)[1†] Quan Liu (刘泉)[2‡] Shou-Wan Chen (陈寿万)[2] Dong-Peng Li (李冬鹏)[3]

[1]School of Mechanics and Optoelectronic Physics, Anhui University of Science and Technology, Huainan 232001, People's Republic of China
[2]School of Physics, Anhui University, Hefei 230601, People's Republic of China
[3]School of Physics and Materials Engineering, Hefei Normal University, Hefei 230601, People's Republic of China

Abstract: Based on the similarity renormalization group (SRG) method with the relativistic mean field (RMF) theory, we diagonalize the Hamiltonian incorporating the tensor coupling effect to explore pseudospin and spin symmetries and their evolutions in Ca isotopes. The restoration of pseudospin symmetry is governed by the competition between H_T^{sl} (the coupling of tensor and spin-orbit term) and H_T^{dw} (the coupling of tensor and Darwin term) via the SRG method. The tensor coupling effect breaks the spin symmetry, primarily driven by H_T^{sl}. It is worth noting that the decrease (increase) of single-particle energy in $\kappa<0$ ($\kappa>0$) states is caused by the H_T^{sl} term in the pseudospin and spin symmetries. The tensor coupling effect drives pseudo(spin) splittings, which highlights the necessity of relativistic approaches with exchange interactions. Compared with the experimental and theoretical results, the tensor coupling effect (fitting the tensor parameters $f(t)=3.1$) induces shell effects at $N=32,34$, which renders these nuclei more magic than predictions by the traditional RMF model. Meanwhile, a more diffuse potential leads to the preservation of PSS in exotic nuclei, as supported by analysis of the mean field potential Σ and its derivative $\Sigma'(r)$.

Keywords: tensor coupling effect, shell evolutions, relativistic symmetries

DOI: 10.1088/1674-1137/ae6a7f **CSTR:**

I. INTRODUCTION

The appearance or vanishing of magic numbers has significant impacts in various fields such as nuclear structure, nuclear interactions, astrophysics, and more. Spin symmetry (SS) and pseudospin symmetry (PSS) have emerged as crucial frameworks for understanding the relativistic nature of nuclear interactions and the (dis)appearance of exotic phenomena [1−8]. The breaking of spin symmetry, namely the spin-orbit splitting in the spin doublets $(n,l,j=l\pm1/2)$, is fundamental for studying magic numbers in nuclear physics [1, 2]. Pseudospin symmetry is a key concept in nuclear structure, observed in the single-particle levels with quantum numbers $(n-1,l+2,j=l+3/2)$ and $(n,l,j=l+1/2)$, which are approximately degenerate and marked as pseudospin doublets $(\tilde{n}=n-1,\tilde{l}=l+1,j=\tilde{l}\pm1/2)$ [3, 4]. In 1997, Ginocchio [5] pointed out that the pseudospin symmetry in nuclei is exactly conserved when the scalar potential $S(r)$ and the vector potential $V(r)$ have the same magnitude but opposite sign. Later, Meng *et al.* extended an approximate condition, showing that pseudospin symmetry is preserved when $d\Sigma(r)/dr=0$ $(\Sigma(r)=S(r)+V(r))$ [9].

The splittings of spin and pseudospin doublets are significant for the reliable description of exotic nuclei, particularly with the addition of tensor coupling. The experimental energy splitting values for a pair of pseudospin doublets ($1\tilde{h}$) reveal the level ordering, which is reproduced by model calculations with tensor coupling (tensor coupling constant is 1.3) [10]. The inclusion of ρ tensor coupling leads to isospin-dependent spin-orbit splittings, influencing the appearance of neutron halo [11]. Contributing to the inclusion of Lorentz tensor ρ-N coupling, the shell closures (58 and 92) have been eliminated [12]. The $Z=64$ subshell was satisfactorily explained by introducing tensor coupling [13]. The relativistic Hartree-Fock-Bogoliubov (RHFB) theory naturally includes the π-meson and ρ-tensor couplings [14], with the prediction of the proton bubble structure in ^{34}Si [15] being confirmed experimentally [16]. The mechanism of halo formation in Ce isotopes [17] successfully explains the experimental results of neutron skin and pseudo-spin orbital (PSO) splittings in the unstable nucleus ^{78}Ni [18].

Received 29 November 2025; Accepted 6 May 2026

* This work was partly supported by the National Natural Science Foundation of China (Grant No. 12475116) and the Scientific Research Foundation for High-Level Talents of Anhui University of Science and Technology (Grant No. 13200400)

† E-mail: sxx@aust.edu.cn
‡ E-mail: sxx@aust.edu.cn

Based on the similarity renormalization group (SRG) method, the tensor coupling effect enlarges (reduces) the energy splittings of spin (pseudospin) in ^{208}Pb [19]. These findings clearly reveal the importance of tensor coupling on shell evolution and relativistic symmetries.

It is known that nuclear force includes central, spin-orbit, tensor components, and more. The tensor force is the tensor component of nuclear force. Under the relativistic scheme, Lorentz tensor couplings exist due to the exchange of vector mesons ω and ρ. Considering only the Hartree terms of these couplings, they are a mixture of central and spin-orbit type components, whereas considering the Fock terms, the tensor type component is automatically involved. Meanwhile, the Fock terms of the Lorentz tensor couplings, namely the π-pseudo-vector and ρ-tensor components, can significantly influence nuclear binding [20−25]. Note that the restoration of PSS and SS is indeed a manifestation of nuclear binding, as deduced from the conservation condition.

Tensor coupling originates in meson exchanges between nucleons in the relativistic framework. Introducing the tensor coupling between the ω meson and the nucleon, the nature of the spin-orbit force is examined in finite nuclei [26]. Including tensor couplings of the ω and ρ mesons, the nucleon spectra of shell models have been improved with the relativistic Hartree approach [27]. The tensor coupling noticeably decreases the PSO splittings, particularly for single-particle levels near the Fermi surface [10]. The tensor interaction can also strongly affect spin symmetry [28]. In Ref. [19], the authors explored the effect of tensor coupling on relativistic symmetries with a focus on single-particle energy.

In $\sum(r)=0$ [5] or $d\sum(r)/dr=0$ [9], there are no bound states, and pseudospin symmetry is always broken in realistic nuclei. Therefore, it is more meaningful to investigate the approximate conservation of pseudospin symmetry in realistic nuclei and the origin of PSS and its breaking mechanism. In Refs. [10, 29], the contribution of tensor coupling to spin and pseudospin symmetry is analyzed by transforming the Dirac Hamiltonian into a Schrödinger-like form. However, calculating the contribution of each component to pseudospin splittings inevitably encountered singularity (the effective mass $M_{-}(r)=0$ at r_0) and the coupling between the operator and its eigenenergy when solving the Schrödinger-like equation for the lower component of the Dirac spinor. Recently, the Dirac Hamiltonian has been transformed into a diagonal form by the SRG method to avoid these defects [30−34]. With the reconstituted SRG method, performing the nonrelativistic expansion of the Dirac equation up to the $1/M^4$ order, single-particle energies and densities are faster convergence than the conventional one [35].

The contribution of each term to pseudospin symmetry and their correlations with the potential shape are examined for all the selected pseudospin doublets [30]. Combining the SRG technique, supersymmetry quantum mechanics, and perturbation theory, the origin of PSS and its breaking mechanism were quantitatively investigated [36, 37]. The origin of relativistic symmetries has been extended in axially deformed nuclei [31, 32]. The role of Coulomb and ρ potentials in the isospin asymmetry of pseudospin splittings has been further investigated [38]. Combining SRG into the relativistic mean field of meson exchange (RMF) and point-coupling (RMFPC) models, the relativistic symmetries depending on isospin and different point-coupling interactions are explored, respectively [33, 34]. Recently, the origin and breaking mechanisms of PSS and SS at new subshells $N=14,16,32$, and 34 isotones are explored by SRG in conjunction with the RMFPC model [39, 40]. The application of the SRG method is very similar to the well-known Foldy-Wouthuysen (FW) transformation [41−43]. Using a novel expansion of the inverse of the Dirac effective mass, the flow equations are solved in the SRG framework in Refs. [44, 45]. Using the similarity renormalization group, Ding *et al.* provide a first-principles explanation for the origin of magic numbers and pseudospin symmetry [46]. The encouraging progress of such work offers a significant way to explore the origin and breaking mechanisms of relativistic symmetries using the SRG method.

With a complete filling of the $Z=20$ shell, the calcium isotopes have shown extreme sensitivity to changes in neutron numbers related to the nuclear shell structure. Signatures of magicity have been observed at $N=20,28$ [47−49]. Considering the recently predicted $N=16$ [15, 50, 51], and discovered $N=32$ and 34 neutron (sub)shell closures [52−56], along with the controversial one at $N=40$ [57−61], the Ca isotopes exhibit more identified magic nuclei in a single isotopic chain.

The high excitation energy of the first 1^+ and 2^+ states in ^{36}Ca, as well as the large neutron-removal spectroscopic factors, indicate a significant gap at $N=16$ [50]. The $N=32,34$ shell closures in ^{52,54}Ca have been claimed from a series of observations relying on the first 2^+ excitation energy [62−64], transition probability [65], mass measurements [52, 53, 66], and neutron knockout cross-section measurements [55]. The measurement of the ^{58,60}Ti excitation energies supports the structure of the potentially doubly magic nucleus ^{60}Ca [67].

Theoretically, the $N=16$ shell gap in ^{36}Ca and ^{24}O are of similar amplitude according to shell model analysis with comparisons to results from two-neutron transfer reactions [51]. Theoretical calculations, including the *ab* initio method [68], the coupled-cluster method [69], shell model [54, 62], and density functional theory [70, 71], also support the emergence of $N=32,34$. With available experimental data, results from data-driven method conclude that ^{60}Ca is doubly magic at a similar level to ^{68}Ni

[58]. Conversely, the possibility for a doubly magic ^{60}Ca is doubted based on shell model calculations [59, 60]. Notably, the RHFB theory naturally includes the π-meson and ρ-tensor couplings and explains the different origins of two successive magic numbers from the perspective of PSS (SS) [56]: the $N=32$ subshell is related to a $\nu 2p$ SO (spin-orbit) splitting, while the persistent subshell of $N=34$ can be related to the $\nu 1\tilde{d}$ PSO splitting. This motivates us to clarify the origin and breaking mechanisms of relativistic symmetries by combining the tensor coupling effect, as well as exploring the possibility of magicity in calcium isotopes.

Although the RMF theory has successfully described the ground state properties of nuclei and reiterated traditional magic numbers, the pure RMF model insufficiently predicts shell gaps for the new magic numbers $N=32,34$, contradicting recent experimental evidence for calcium isotopes. This discrepancy highlights the need for a self-consistent framework that combines other coupling effects. Our study addresses this issue by combining SRG with RMF and the tensor coupling effect on relativistic symmetries. In this paper, we utilize the RMF model with the SRG method, termed the RMF-SRG method. The paper is structured as follows: Section II introduces the theoretical formalism. Section III presents detailed discussions on the contribution of the tensor coupling effect to shell evolution and relativistic symmetries. Section IV provides a brief summary.

II. THE SRG METHOD

The most popular RMF model is based on the finite-range meson-exchange representation, according to which nucleons are viewed as Dirac particles interacting via the exchange of various mesons and photons. The connection between the pseudospin symmetry and RMF theory [72−75] was first identified to approximately explain such a special ratio between the strengths of the spin-orbit and orbit-orbit interactions [76]. By analyzing Ca isotopes, it is shown, in particular, that an enhancement of the new magic numbers may be predicted within mean field calculations by including more elaborate nuclear effective interactions, like the tensor coupling effect [10]. The following Lagrangian density can be written as [19, 27]

$$\mathcal{L}=\mathcal{L}_{\mathcal{F}}+\mathcal{L}_{I}, \tag{1}$$

where $\mathcal{L}_{\mathcal{F}}$ is the Lagrangian density for free nucleons, mesons (σ, ω, and ρ), and photons,

$$\begin{aligned}\mathcal{L}_{\mathcal{F}}=&\bar{\psi}(i\gamma^{\mu}\partial_{\mu}-M)\psi+\frac{1}{2}\partial_{\mu}\sigma\partial^{\mu}\sigma-\frac{1}{2}m_{\sigma}^{2}\sigma^{2}\\&-\frac{g_2}{3}\sigma^{3}-\frac{g_3}{4}\sigma^{4}-\frac{1}{4}\Omega_{\mu\nu}\Omega^{\mu\nu}+\frac{1}{2}m_{\omega}^{2}\omega_{\mu}\omega^{\mu}\\&-\frac{1}{4}\vec{R}_{\mu\nu}\vec{R}^{\mu\nu}+\frac{1}{2}m_{\rho}^{2}\vec{\rho}_{\mu}\vec{\rho}^{\mu}-\frac{1}{4}F_{\mu\nu}F^{\mu\nu}.\end{aligned} \tag{2}$$

Here, M is the nucleon mass. The field tensors for the vector mesons and photons are defined as follows:

$$\begin{aligned}\Omega_{\mu\nu}&=\partial_{\mu}\omega_{\nu}-\partial_{\nu}\omega_{\mu},\\\vec{R}_{\mu\nu}&=\partial_{\mu}\vec{\rho}_{\nu}-\partial_{\nu}\vec{\rho}_{\mu}-g_{\rho}(\vec{\rho}_{\mu}\times\vec{\rho}_{\nu}),\\F_{\mu\nu}&=\partial_{\mu}A_{\nu}-\partial_{\nu}A_{\mu}.\end{aligned} \tag{3}$$

The interaction between nucleons via the exchange of mesons and photons can be expressed in the Lagrangian density $\mathcal{L}_{I}$, which takes the following form:

$$\begin{aligned}\mathcal{L}_{I}=\bar{\psi}[&-g_{\sigma}\sigma-g_{\omega}\gamma^{\mu}\omega_{\mu}-g_{\rho}\gamma^{\mu}\vec{\tau}\vec{\rho}_{\mu}-e\frac{1-\tau_3}{2}\gamma^{\mu}A_{\mu}\\&-\frac{f_{\omega}}{2M}\gamma^{\mu\nu}\Omega_{\mu\nu}-\frac{f_{\rho}}{2M}\gamma^{\mu\nu}\vec{\tau}\vec{R}_{\mu\nu}]\psi.\end{aligned} \tag{4}$$

Here, $\gamma^{\mu\nu}=\frac{i}{2}[\gamma^{\mu},\gamma^{\nu}]$. τ is the isospin operator of the nucleon and τ_3 is its third component. $g_{\sigma},g_{\omega},g_{\rho}$, and $e^2/4\pi=1/137$ are the coupling strengths for the σ,ω,ρ mesons and for the photon, respectively. f_{ω} and f_{ρ} are the tensor-coupling strengths of vector mesons ω and ρ, respectively. m_{σ},m_{ω}, and m_{ρ} are the masses of the corresponding mesons. In the interaction Lagrangian density Eq. (4), we consider the Lorentz σ-scalar, ω-vector, ρ-vector, ρ-tensor, ω-tensor, and photon-vector couplings.

In terms of the classical variation principle, one can derive the Euler-Lagrange equation.

$$\partial_{\mu}\frac{\partial\mathcal{L}}{\partial(\partial_{\mu}\phi)}-\frac{\partial\mathcal{L}}{\partial\phi}=0 \tag{5}$$

By taking $\phi=\psi$ and considering the mean field approximation, the meson fields are static, and only the time-like component is considered. Therefore, we have the following:

$$\begin{aligned}i\frac{\partial\psi}{\partial t}=&[-i\vec{\alpha}\nabla+\beta(M+g_{\sigma}\sigma)+g_{\omega}\omega_0+g_{\rho}\tau_3\rho_0+e\frac{1-\tau_3}{2}A_0\\&-i\frac{f_{\omega}}{M}\beta\vec{\alpha}\cdot\nabla\omega_0-i\frac{f_{\rho}}{M}\tau_3\beta\vec{\alpha}\cdot\nabla\rho_0]\psi.\end{aligned} \tag{6}$$

From the above equation, the Dirac Hamiltonian is obtained as

$$\begin{aligned}H=&\vec{\alpha}\cdot\vec{p}+\beta(M+g_{\sigma}\sigma)+g_{\omega}\omega_0+g_{\rho}\tau_3\rho_0+e\frac{1-\tau_3}{2}A_0\\&+\frac{1}{M}\beta\vec{\alpha}\cdot\vec{p}(f_{\omega}\omega_0+\tau_3 f_{\rho}\rho_0)\end{aligned} \tag{7}$$

Here, $\vec{p}$ and $\vec{p'}$ are fundamentally different: the former acts on the single particle states while the latter is supposed to act on the propagators in the meson fields (ω_0 and ρ_0). These correspond to the single particle momentum and momentum transfer, respectively. For simplicity, the above Hamiltonian can be written as

$$H = \vec{\alpha}\cdot\vec{p} + V + \beta(M+S) + \frac{1}{M}\beta\vec{\alpha}\cdot(\vec{p'}u), \tag{8}$$

where V, S, and u are the vector, scalar [72, 74], and tensor potentials [19], respectively. Here, the vector mesons we are considering are the isoscalar ω mesons and isovector vector ρ mesons. Therefore, the Lorentz ω-tensor and ρ-tensor are introduced. The tensor force components carried by the π-pseudo-vector couplings can significantly change the evolution of the single-particle orbits [56, 77], which is not considered here.

$$\begin{aligned} S &= g_\sigma\sigma, \\ V &= g_\omega\omega_0 + \tau_3 g_\rho\rho_0 + e\frac{1-\tau_3}{2}A_0, \\ u &= f_\omega\omega_0 + \tau_3 f_\rho\rho_0. \end{aligned} \tag{9}$$

f_ω and f_ρ are the tensor-coupling strengths of vector mesons. Assuming $\frac{f_\omega}{g_\omega} = \frac{f_\rho}{g_\rho} = f_t$, the tensor component simplifies to:

$$u = f_t(g_\omega\omega_0 + \tau_3 g_\rho\rho_0). \tag{10}$$

For the neutron ($\tau_3 = 1$), $u = f_t$V. For the spherical nuclei, the Dirac spinor has the following form:

$$\begin{aligned} \psi &= \frac{1}{r}\begin{pmatrix} iF(r)Y_{jlm}(\vartheta,\varphi) \\ -G(r)Y_{j\tilde{l}m}(\vartheta,\varphi) \end{pmatrix}, \\ j &= l + \frac{1}{2} = \tilde{l} - \frac{1}{2}. \end{aligned} \tag{11}$$

Then, the Dirac equation can be expressed as

$$\begin{aligned} &\begin{pmatrix} V+S+M & -\frac{d}{dr} - \frac{U}{M} + \frac{\kappa}{r} \\ \frac{d}{dr} + \frac{\kappa}{r} - \frac{U}{M} & V-S-M \end{pmatrix}\begin{pmatrix} F(r) \\ G(r) \end{pmatrix} \\ &= \varepsilon\begin{pmatrix} F(r) \\ G(r) \end{pmatrix}, \end{aligned} \tag{12}$$

where $U = \frac{du}{dr}$. Utilizing Wegner's formulation of the SRG [78], the H operator transforms into a diagonal form. The initial Hamiltonian H is transformed by the unitary operator $U(l)$ according to

$$H(l) = U(l)HU^\dagger(l), \quad H(0) = H, \tag{13}$$

where l is a flow parameter. By differentiating Equation (13), the flow equation is defined as:

$$\frac{d}{dl}H(l) = \left[\eta(l), H(l)\right], \tag{14}$$

with the generator

$$\eta(l) = \frac{dU(l)}{dl}U^\dagger(l) = -\eta^\dagger(l). \tag{15}$$

Based on Wegner's theory, the form $\eta(l) = [H_d(l), H(l)]$ is a suitable choice, where $H_d(l)$ is the diagonal part of $H(l)$ [78]. Therefore, it is appropriate to further select $\eta(l) = [\beta M, H(l)]$ [79]. The Hamiltonian $H(l)$ can be expressed as a sum of an even operator $\epsilon(l)$ and an odd operator $o(l)$:

$$H(l) = \epsilon(l) + o(l). \tag{16}$$

Following the commutation relations of the operators, the evenness or oddness of $\epsilon(l)$ and $o(l)$ can be defined by $\epsilon(l)\beta = \beta\epsilon(l)$ and $o(l)\beta = -\beta o(l)$, respectively. Then, putting Eqs. (15) and (16) into Eq. (14) gives

$$\begin{aligned} \frac{d\epsilon(l)}{dl} &= 4M\beta o^2(l), \\ \frac{do(l)}{dl} &= 2M\beta[o(l), \epsilon(l)]. \end{aligned} \tag{17}$$

Eq. (17) can be solved by perturbation within $1/M$. For simplicity, we introduce a dimensionless flow parameter $\lambda = lM^2$ to diagonalize the Hamiltonian. Beginning with the zeroth-order term, the expansion of $\varepsilon(\lambda)/M$ in a series of $1/M$ results in the following equations:

$$\frac{1}{M}\varepsilon(\lambda) = \sum_{i=0}^{\infty}\frac{1}{M^i}\varepsilon_i(\lambda). \tag{18}$$

The expansion of $o(\lambda)/M$ starts with the first order.

$$\frac{1}{M}o(\lambda) = \sum_{j=1}^{\infty}\frac{1}{M^j}o_j(\lambda). \tag{19}$$

Differentiation Eqs. (18) and (19) yields the equations:

$$\frac{d\varepsilon_n(\lambda)}{d\lambda} = 4\beta\sum_{k=1}^{n-1} o_k(\lambda)o_{n-k}(\lambda),$$
$$\frac{do_n(\lambda)}{d\lambda} = -4o_n(\lambda) + 2\beta\sum_{k=1}^{n-1}[o_k(\lambda),\varepsilon_{n-k}(\lambda)]. \quad (20)$$

The solutions of the above equations are obtained as:

$$\varepsilon_n(\lambda) = 4\beta\int_0^\lambda d\lambda'\sum_{k=1}^{n-1} o_k(\lambda')o_{n-k}(\lambda') + \varepsilon_n(0),$$
$$o_n(\lambda) = 2\beta e^{-4\lambda}\int_0^\lambda d\lambda'\sum_{k=1}^{n-1}[e^{4\lambda'}o_k(\lambda'),\varepsilon_{n-k}(\lambda')] + o_n(0)e^{-4\lambda}. \quad (21)$$

Combining with the present Hamiltonian system, the initial condition is presented as:

$$\varepsilon_0(0) = \beta, \varepsilon_1(0) = \beta S + V, \epsilon_n(0) = 0 (n \geq 2),$$
$$o_1(0) = \vec{\alpha}\cdot\vec{p}, o_n(0) = 0 (n \geq 2). \quad (22)$$

From the above equations, we can acquire

$$\varepsilon_0(\lambda) = \beta,$$
$$\varepsilon_1(\lambda) = \beta S + V,$$
$$o_1(\lambda) = o_1(0)e^{-4\lambda}, \quad (23)$$

and $o_n(\lambda)$ exponentially goes to zero as $\lambda \to \infty$. Thus, the diagonalized Dirac operator becomes

$$\varepsilon(\infty) = M\epsilon_0(\infty) + \epsilon_1(\infty) + \frac{1}{M}\epsilon_2(\infty) + \frac{1}{M^2}\epsilon_3(\infty) + \frac{1}{M^3}\epsilon_4(\infty) + ... = \begin{pmatrix} H_P + M & 0 \\ 0 & -H_P^C - M \end{pmatrix}, \quad (24)$$

where

$$H_P = H_O + H_T. \quad (25)$$

H_O is an operator describing the Dirac particle without a tensor coupling.

$$H_O = H_n + H_d + H_c + H_k + H_w, \quad (26)$$

where the expressions for these five Hermitian components are

$$H_n = \Sigma(r) + \frac{p^2}{2M},$$
$$H_d = -\frac{(S\,p^2 - S'\frac{d}{dr})}{2M^2} + \frac{S(S\,p^2 - 2S'\frac{d}{dr})}{2M^3},$$
$$H_c = (2S - M)\frac{\kappa}{r}\frac{\Delta'}{4M^3},$$
$$H_k = -\frac{p^4}{8M^3},$$
$$H_w = \frac{\Sigma''}{8M^2} - \frac{\Sigma'^2 - 2\Sigma'\Delta' + 4S\Sigma''}{16M^3}. \quad (27)$$

H_n represents the operator describing a Dirac particle in the nonrelativistic limit. H_d and H_c correspond to the dynamical effect and the spin-orbit interaction, respectively. H_k reflects the relativistic modification of kinetic energy. H_w denotes the Darwin term. The operator H_P describes a Dirac particle with $p^2 = -\frac{d^2}{dr^2} + \frac{\kappa(\kappa+1)}{r^2}$, where κ is a good quantum number defined as $\kappa = \pm(j+1/2)$. H_P^C (for Dirac antiparticles [7, 80]) is the charge-conjugation of H_P with $p^2 = -\frac{d^2}{dr^2} + \frac{\kappa(\kappa-1)}{r^2}$. $\Sigma(r) = S(r) + V(r)$ and $\Delta(r) = S(r) - V(r)$ denote the combinations of the scalar potential $S(r)$ and the vector potential $V(r)$. The primes and double primes in H_P denote the first-order and second-order derivatives with respect to r, respectively. The singularity vanishes in every component of Eq. (25), and all the terms are Hermitian in H_P. The total tensor coupling operator H_T can be separated into the coupling of the tensor and spin-orbit term H_T^{sl} and the Darwin term H_T^{dw}, respectively.

$$H_T = H_T^{sl} + H_T^{dw}, \quad (28)$$

where

$$H_T^{sl} = -\frac{U}{M^2}\frac{\kappa}{r} + \frac{S\,U}{M^3}\frac{\kappa}{r}, \quad (29)$$

$$H_T^{dw} = \frac{2MU' - 2S\,U' + 2U^2 + \Delta' U}{4M^3}. \quad (30)$$

In Ref. [19], spin symmetry is exact for a Dirac particle when $\Delta' = 0$ and $U = 0$. Unlike the Dirac Hamiltonian in Ref. [79], the H_T^{sl} and H_T^{dw} terms originate from the tensor coupling.

III. NUMERICAL DETAILS AND RESULTS

To explore the origin and broken mechanism of relativistic symmetries in shell evolution, the energy splittings for (pseudo)spin doublets in selected even-even calcium isotopes are shown with(out) the tensor coupling ef-

fect by the RMF-SRG method. Here, ^{36,40,48,52,54,60}Ca are considered as dual magic nuclei, despite questions about the robustness of $N=40$ in ^{60}Ca [60]. The energy splittings contributed by H_O are independent of the tensor coupling, and every component from H_O has a similar contribution to PSS (SS) as discussed in Refs. [30−33].

A. Pseudospin symmetry in Ca isotopes with tensor coupling effect

In Refs. [51, 81], ^{36}Ca may be a better closed-subshell nucleus at $N=16$, which is related to the pseudospin energy splitting of the $\nu 1\tilde{p}$ ($\nu 2s_{1/2}$, $\nu 1d_{3/2}$) doublet. With the inclusion of the tensor coupling effect H_T (including the coupling between the tensor and Darwin term H_T^{dw}, and the spin-orbit term H_T^{sl}) added to the H_O term, the total pseudospin energy splitting term (H_O+H_T) changes monotonically for doublets $\nu 1\tilde{p}$ and $\nu 1\tilde{d}$ ($\nu 2p_{3/2}$, $\nu 1f_{5/2}$) as they vary with the strength of tensor coupling $f(t)$ in Figs. 1 and 2. By tuning $f(t)$ up to one, H_T^{sl} and H_T^{dw} become comparable to the spin-orbit coupling or the dynamical effect [19]. In Fig. 1, the restoration of pseudospin symmetry depends on the competition between H_T^{sl} and H_T^{dw}. Due to the near cancellation between H_T^{sl} and H_T^{dw} in Fig. 1, the tiny contribution is smaller for the $N=16$ subshell [51]. Although single-particle energies are difficult to determine experimentally, state-of-the-art shell model calculations underestimate the size of the $N=16$ gap in ^{36}Ca by 840 keV [51]. In the present model, the tensor coupling effect alone is insufficient to provide an enhancement of the $N=16$ gap. Incorporating additional interactions may help improve the agreement with the experimental observations [51].

^{40}Ca is a spin saturated nucleus and is famous as the *LS* doubly closed nucleus. Comparing with the experimental data [82−85], the negative energy splitting term H_O with the destructive behavior of H_T for ^{40}Ca is shown in Fig. 1. The $\nu 2s_{1/2}$ orbit lies below its PSS partner $\nu 1d_{3/2}$ and it may go up and down because of the unoccupied $\pi 1d_{3/2}$ orbit in Ref. [87], which indicates a change in energy splitting. As the splitting energy is negative [87], the H_T term may theoretically have a destructive behavior for this doublet. For ^{48}Ca in Fig. 1, there is an inversion ($\nu 2s_{1/2}$, $\nu 1d_{3/2}$) in the H_O term. The energy splitting for the H_T term shows a distinct enhancement of 1.33 MeV at $f(t)=1$ in ^{48}Ca in Fig. 1. H_T^{sl} and H_T^{dw} terms give opposite contributions to $\nu 1\tilde{p}$ pseudospin splittings with different amplitudes; therefore, the total tensor coupling term H_T plays a detrimental role in ^{48}Ca when compared with the corresponding experimental and theoretical single-particle energies [48, 86, 88]. For ^{52}Ca, the H_T term causes slight changes in energy splittings. For the nuclei ^{54,60}Ca, the energy splittings obtained with and without the tensor effect coupling are nearly identical, so the tensor coupling effect is not active here. It is noted that H_T^{sl} for the $\kappa<0$ states is negative, but for the $\kappa>0$ states is positive. Therefore, H_T^{sl} is always negative in the energy splittings of all selected pseudospin doublets.

Compared with the $\nu 1\tilde{p}$ doublet, another pseudospin

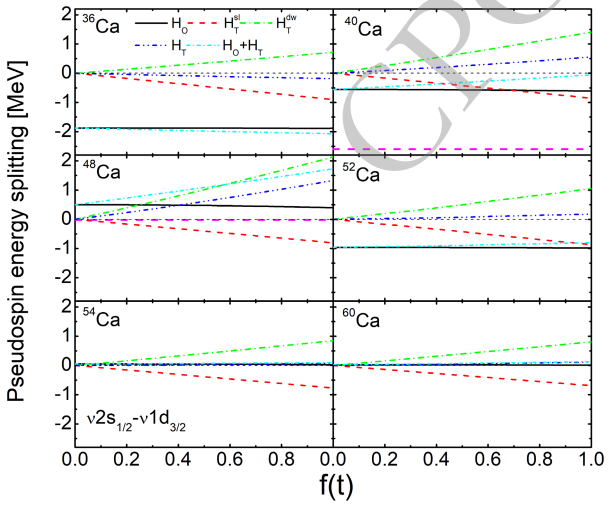

Fig. 1. (Color online) Variations of energy splittings with the tensor coupling strength $f(t)$ for neutron pseudospin doublet ($\nu 2s_{1/2}$, $\nu 1d_{3/2}$) in selected Ca isotones. The black (solid), red (dashed), green (dash-dot), and blue (dash-dot-dot) lines in each subfigure represent the splittings contributed by the term describing the Dirac particle: without tensor coupling H_O, the coupling between the spin-orbit and the tensor H_T^{sl}, the coupling between the Darwin term and the tensor H_T^{dw}, and the total tensor coupling term H_T, respectively. The cyan (short-dash-dot) line denotes the total pseudospin energy splitting term H_O+H_T. The magenta (dashed) line represents the experimental values for ^{40,48}Ca [48, 82−86].

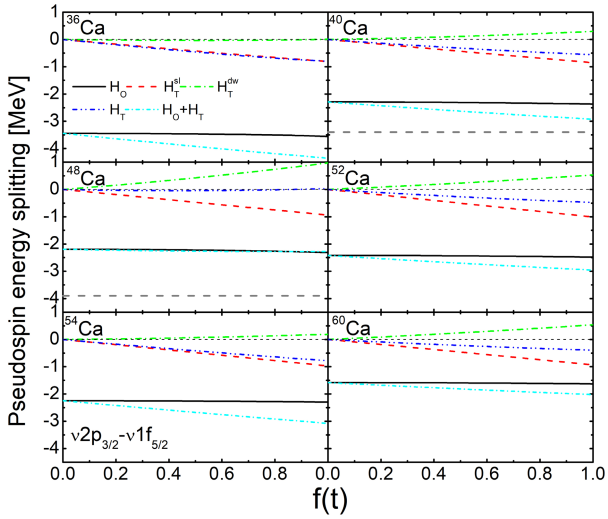

Fig. 2. (Color online) The same as Fig. 1, but for the neutron pseudospin doublet ($\nu 2p_{3/2}$, $\nu 1f_{5/2}$). The gray (dashed) line represents the experimental values also for ^{40,48}Ca [83−85, 89, 90].

doublet $\nu 1\tilde{d}$ ($\nu 2p_{3/2}$ and $\nu 1f_{5/2}$) with higher orbital angular momentum shows the variation of energy splittings with the tensor coupling coefficient $f(t)$ in Fig. 2. In ^{36}Ca, the H_T^{dw} term presents tiny contributions to H_T, meaning that the H_T^{sl} term primarily governs the total tensor coupling term H_T, resulting in a maximum in pseudospin energy splittings. Compared with the single particle data for $\nu 1\tilde{d}$ in ^{40}Ca [83−85, 89, 90], the tensor coupling effect should be included for PSS. For the $\nu 1\tilde{d}$ doublet of ^{48}Ca, the H_T^{dw} and H_T^{sl} terms have approximately equal magnitude and opposite sign with the tensor coupling coefficient $f(t)$. Consequently, the net tensor coupling effect is almost invisible. However, the energy splittings of $\nu 1\tilde{d}$ cannot support the appearance of $N = 32, 34$ subshells in Fig. 2. One can notice that the shell evolutions are also related to the spin doublet $\nu 2p$ in Fig. 3. Compared with other isotopes, the pseudospin energy splitting in ^{60}Ca is small, and the tensor coupling effect enlarges the splitting value, a trend that aligns with results from the SKX functional [58] as the tensor coupling strength $f(t)$ increases. Notably, the H_T^{sl} term is negative and further enhances its magnitude, as illustrated in Fig. 2.

B. Spin symmetry in Ca isotopes with tensor coupling effect

The variations of spin energy splittings with the strength of the tensor coupling $f(t)$ for all selected neutron spin doublets are displayed in Figs. 3 and 5 ~ 7. The position of the spin doublet $\nu 2p$ is close to the Fermi surface in Fig. 3. The total energy splitting term (H_O+H_T) with $f(t)$ exhibits a trend similar to H_T. It is noticed that the coupling of the tensor and Darwin term H_T^{dw} is sensitive to the tensor coefficient $f(t)$ in ^{36,40}Ca, indicating that these two terms (H_T^{sl} and H_T^{dw}) largely cancel each other out, unlike the other isotopes in Fig. 3. This suggests the minimal significance of the H_T^{dw} term in the ^{48,52,54,60}Ca isotopes, where the H_T^{sl} term plays an important role, rather than the H_T^{dw} term. Such a tensor coupling contribution is expected to induce an increase in the spin energy splittings of the $2p$ doublet, and the single-particle gaps obtained for ^{40,48}Ca are close to the experimental values (2 MeV) [83−85, 89, 90]. Meanwhile, the theoretical predictions for ^{60}Ca are approaching 2 MeV [58, 60].

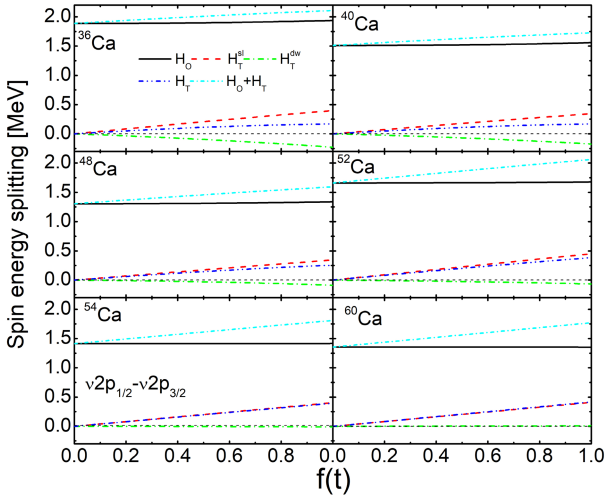

Fig. 3. (Color online) The same as Fig. 1, but for the neutron spin doublet ($\nu 2p_{1/2}$, $\nu 2p_{3/2}$).

With the increasing neutron number, the spin energy splittings from H_O decrease from ^{36}Ca to ^{48}Ca in Fig. 3. The discontinuity of the isospin effect suggests that there may be new magic numbers related to the spin doublet $\nu 2p$ in ^{52}Ca. A single neutron excitation across the $N = 32$ subshell closure ($\nu 2p_{3/2} \rightarrow \nu 2p_{1/2}$) is mainly responsible for the first excited 2^+ state in ^{52}Ca. An enhancement of the magicity of ^{52}Ca may be predicted by including the like-particle contribution generated by the tensor force [71]. The experimental evidence for the $N = 32$ closure is compelling (approximately 2.6 MeV) [64, 91]. The magnitude of the $N = 32$ subshell is well documented by shell-model calculations performed in the sdpf model space using the SDPF-MU effective interaction (approximately 2.4 MeV) [62].

Although one cannot perfectly reproduce the gap value of the new magic number $N = 32$ in the experiments [64, 91], the gap in ^{52}Ca is related to the large spin splittings of the $\nu 2p$ orbits [56], and calculations with beyond mean field theory also support the opening of the $N = 32$ subshell in Ca isotopes [92]. For $\nu 2p$ doublets in Fig. 3, the total energy splitting in ^{52}Ca is 2.06 MeV with a tensor coupling coefficient $f(t) = 1$. According to Ref. [56], the effect of the Lorentz PV and T couplings in ^{52}Ca is shown to be dominant in RHFB theory (2.72 MeV is obtained in RHFB-PKA1) [56]. Comparing the experimental data with the theoretical calculation of the $\nu 2p$ SO splitting ($N = 32$), 2.06 MeV seems insufficient to predict the new magic number $N = 32$ in Fig. 3. Therefore, a stronger tensor coupling effect is required to accurately reproduce single-particle evolutions. For ^{60}Ca, the two terms (H_O, H_O+H_T) remain smaller, indicating that better spin symmetry tends to be preserved in exotic nuclei close to the Fermi surface.

As shown in Fig. 4, the global enhancements of the single particle levels and gaps are visible due to the tensor coupling effect. However, the increases in $1d_{3/2}$, $2p_{1/2}$, and $1f_{5/2}$ are greater than their comparators, as can be seen from the non-parallel dashed line slopes. For the pseudospin doublet $\nu 1\tilde{p}$, the H_T^{sl} term acts in opposite directions on the $2s_{1/2}$ state ($\kappa = -1$) and $1d_{3/2}$ ($\kappa = 2$). Meanwhile, the H_T^{dw} term in $2s_{1/2}$ is larger than that of $1d_{3/2}$, implying that the tensor coupling effect alone is not able to adequately reproduce the $N = 16$ gap in Fig. 4(a).

Recently, the underlying mechanism of the new magicity $N = 32, 34$ can be explained by the strong couplings

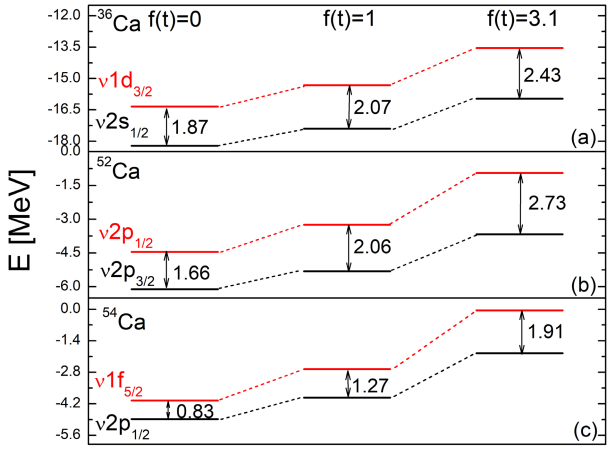

Fig. 4. (Color online) Variation of single-particle energy with the tensor coupling strength $f(t)=0,1,3.1$. Subfigures (a), (b), and (c) represent $N=16,32,34$ subshells, respectivelyB

between the "Dirac inversion partners" [77]. In Figs. 4(b) and (c), it is obvious that the stronger enhancement of the subshell gaps is obtained in ^{52,54}Ca. Under the assumption of vector dominance, there exist constraints of nucleon electromagnetic form factors on the value f_v ($f(t)$) in free space. Therefore, smaller values of f_v ($f(t)$) are favored. However, the mean field parameters obtained from fitting to finite nuclei can be very different from the free space [26]. In Ref. [26], the range of f_v ($f(t)$) is 0 to 3.0. Thus, to achieve satisfactory results with experimental and theoretical outcomes [56, 62, 64, 91], the tensor coupling coefficient needs to reach $f(t)=3.1$ to reproduce the $N=32$ gap in Fig. 4. In fact, the H_T^{dw} term contributes similarly to $2p_{1/2}$ and $2p_{3/2}$ states, while the H_T^{sl} term is negative for $2p_{3/2}$ in ^{52}Ca. Therefore, increasing the coupling strength to 3.1 can appropriately describe the energy gap, which is in good agreement with the results obtained from RHFB-PKA1 [56].

From the measurement of the 2_1^+ state, the excitation energy in ^{54}Ca was found to be only ~ 500 keV below that in ^{52}Ca [54], supporting a possible new $N=34$ shell closure that is appearing between $\nu 2p_{1/2}$ ($\kappa=1$) and $\nu 1f_{5/2}$ ($\kappa=3$) states. Compared with the κ and H_T^{sl} term for $1f_{5/2}$, its partner $2p_{1/2}$ has smaller κ and H_T^{sl} terms. As $f(t)$ increases, the $N=34$ subshell is significantly enhanced. Fitting $f(t)=3.1$, the energy gap for $N=34$ is 1.91 MeV. Hagen *et al.* predicted the excitation energy of 2_1^+ in ^{54}Ca at 1.9 MeV [69], and Steppenbeck *et al.* [54] observed 2043(19) keV in ^{54}Ca. The gaps increase from 1.66 to 2.73 MeV for ^{52}Ca and from 0.83 to 1.91 MeV for ^{54}Ca, reinforcing the magic character for the two isotopes and demonstrating that the inclusion of the tensor effect in single-particle energy shifts the predicted gaps toward the experimental results. However, it is noted that the possible $N=34$ magic number is less marked in the neighboring isotopes like ^{52}Ca in Fig. 4. This situation also occurs with RHFB-PKA1, due to the near cancellation between the central and the rank-2 tensor components of the Lorentz PV and T couplings [56].

In Figs. 3 and 5, the energy splittings contributed by H_T^{sl} in the same nuclei are more sensitive to $f(t)$ for the spin doublets with smaller main quantum number n. These lead to a pattern of total spin energy splitting that is similar to that of H_T^{sl}. Except for ^{36}Ca in Figs. 5 ~ 7, the H_T term increases faster for the doublets with larger orbital angular momentum in the same nuclei with main quantum number $n=1$. The experimental spin energy splitting for ^{40}Ca is only 3 MeV [85], so the tensor coupling effect should not be considered in this nucleus in Fig. 5. The amplitude of the H_T term in $\nu 1d$ ($\nu 1d_{3/2}$, $\nu 1d_{5/2}$) is comparable to that in the $\nu 1f$ ($\nu 1f_{5/2}$, $\nu 1f_{7/2}$), suggesting a new subshell is about to appear in ^{36}Ca involving a pair of spin doublets.

In Fig. 6, the largest spin energy splitting of 8.12 MeV is observed in ^{36}Ca, favoring the single-particle energy predicted by the shell model with the $sdpf-u-mix$ interaction [51]. The $\nu 1d$ spin doublet is related to the occurrence of new subshells $N=14,16$, which predict the next shell closure of the Ca isotopes in the doubly magic and unbound ^{34}Ca [51]. When the tensor coupling effect is included in the H_O term, the total energy splitting of the doublet $\nu 1d$ adds up to 7.2 MeV in ^{40}Ca, which is close to the experimental value [86]. However, compared with experimental [84–86] and theoretical values (the correlations beyond the mean field) [93], the spin energy splitting of the doublet $\nu 1f$ in ^{40}Ca is too large with the tensor coupling. Notice that we only take the experimental data as a reference due to the limits of mean field theory. In the present calculations, the correlations beyond the mean field [92–94], such as the particle-vibration couplings [93, 95], are not taken into account.

The $\nu 1f$ doublet is related to the persistence of traditional magic numbers $N=28$ (the $N=28$ gap is driven by

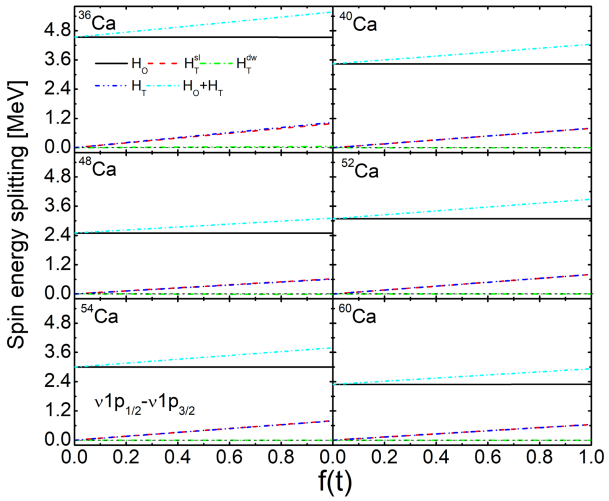

Fig. 5. (Color online) The same as Fig. 1, but for the neutron spin doublet ($\nu 1p_{1/2}$, $\nu 1p_{3/2}$).

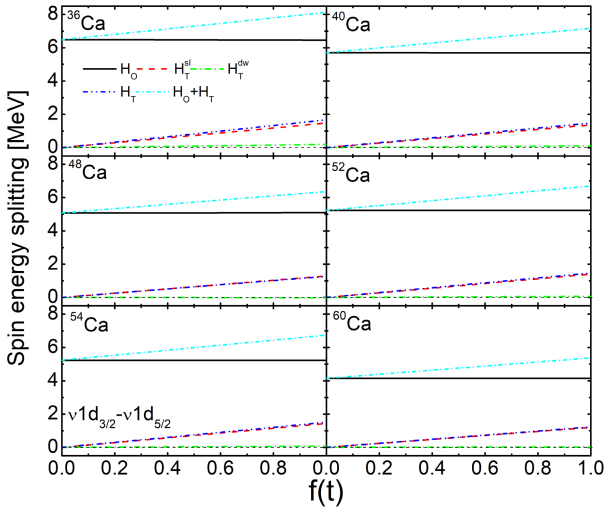

Fig. 6. (Color online) The same as Fig. 1, but for the neutron spin doublet ($\nu 1d_{3/2}$, $\nu 1d_{5/2}$).

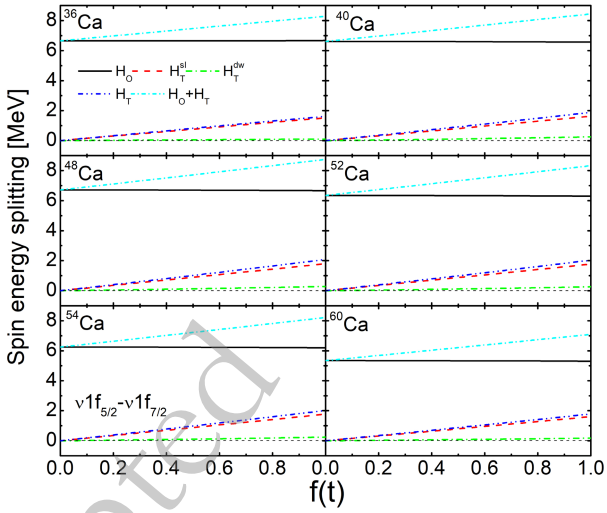

Fig. 7. (Color online) The same as Fig. 1, but for the neutron spin doublet ($\nu 1f_{5/2}$, $\nu 1f_{7/2}$).

the shell gap between the $\nu 2p_{3/2}$ and $\nu 1f_{7/2}$ states) and the new subshells $N = 32, 34$ in Fig. 7. These strongly enlarge the energy splittings in the $\nu 1f$ spin doublet among other spin doublets in ^{48,52,54}Ca. The value of 8.75 MeV ($f(t) = 1$) in ^{48}Ca provides the correct behavior with respect to the experimental value of 8.7 MeV [83, 84, 89] in $\nu 1f$, also supporting the traditional number $N = 28$. With the tensor coupling effect on shell evolution, the trend of energy splittings of this spin doublet with increasing neutron numbers is basically consistent with those of RHFB-PKA1 [56]. Mainly caused by H_T^{sl} in Figs. $3, 5 \sim 7$, the total tensor coupling always destroys the spin symmetry with the selected calcium isotopes. The H_T^{sl} term for the $\kappa < 0$ states is negative and for the $\kappa > 0$ states is positive, resulting in a positive value for the energy splittings of all selected spin doublets. Although a sizable energy splitting exists in ^{60}Ca near the Fermi surface [94], the minimal energy splittings (≈ 7 MeV in Fig. 7) occur in ^{60}Ca among other isotopes, indicating that better spin symmetry is preserved in neutron-rich nuclei. In this case, the tensor coupling effect cannot be ignored when involving relativistic symmetries.

C. The PSS conservation in Ca isotopes

To elucidate the mechanism underlying the improved PSS in exotic nuclei, we examine the mean field potential $\Sigma(r)$ and its derivative $\Sigma'(r)$. The pseudospin-orbit potential depends on the derivative of the sum of the scalar and vector potentials, which has the PSS conservation in real nuclei, namely $d(V+S)/dr = 0$ [9], as shown in Fig. 8. In Fig. 8(a), the mean field potentials of all selected isotopes tend to decrease in absolute value, resulting in their potential derivative $\Sigma'(r)$ being positive in Fig. 8(b). The potential of ^{36}Ca is the deepest among other isotopes, and its potential derivative is also larger near the nuclear surface, corresponding to the worse PSS in Figs. 1 and 2,

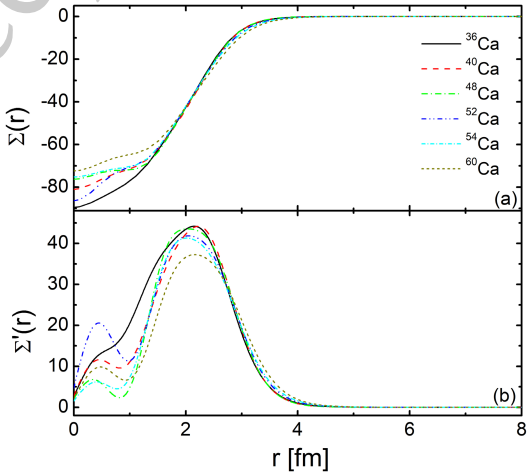

Fig. 8. (Color online) The mean field potential $\Sigma(r)$ (a) and its derivative $\Sigma'(r)$ (b) with respect to r for the selected neutron isotopes.

indicating the possibility of an $N = 16$ subshell. $\Sigma'(r)$ reaches a maximum near the nuclear surface in Fig. 8(b), showing that the larger pseudospin energy splitting exists in ^{52}Ca. With the increasing of r, the neutron potential for ^{60}Ca is central-flat, leading to a smaller derivative and implying a well-preserved PSS in ^{60}Ca. These results demonstrate that better pseudospin symmetry is more likely to be conserved in exotic nuclei. Meanwhile, $\Sigma'(r)$ of all examined calcium isotopes becomes small (~ 0) and its peak shifts from left to right with increasing r. This phenomenon is due to the fact that the improvement of PSS is favored to retain in a more diffuse potential.

IV. SUMMARY

Utilizing the similarity renormalization group with the RMF theory, the tensor coupling effect has been sys-

tematically examined on relativistic symmetries for calcium isotopes. The Dirac Hamiltonian with tensor coupling has been transformed into a diagonal form, and the operator reflecting the tensor coupling can be expressed as the coupling of the tensor and spin-orbit term H_T^{sl} and Darwin term H_T^{dw}.

For all the selected pseudospin doublets in Ca isotopes, the restoration of PSS is governed by the competition between H_T^{sl} and H_T^{dw}, which are comparable to those from the spin-orbit coupling or the dynamical effect. The H_T^{sl} term is always negative among the examined pseudospin splittings, leading to reduced (increased) single particle energy for $\kappa<0$ ($\kappa>0$) states. The magic number $N=16$ is closely associated with the largest energy splitting in the $\nu 1\tilde{d}$ doublet of ^{36}Ca. The restoration (broken) of PSS at ^{60}Ca (^{36,52}Ca) is correlated with the self-consistent mean field potentials $\Sigma(r)$, along with their derivative $\Sigma'(r)$. As the peak of $\Sigma'(r)$ diminishes and shifts rightward, the potential $\Sigma(r)$ broadens and disperses, and the enhanced preservation of PSS is more likely to occur in exotic nuclei with highly diffuse potentials.

The tensor coupling effect predominantly breaks spin symmetry, with the primary contribution stemming from the H_T^{sl} term. The H_T^{sl} term is always positive among the examined spin doublets for the same reason as for PSS. As the main quantum number n increases, the total (tensor) spin splittings become smaller in the same nuclei. Improved SS is more frequently observed in exotic nuclei, particularly for single particle states near the Fermi surface. Comparing with the experimental and theoretical results, it is found that the tensor coupling effect plays an important role in shell evolutions, especially in regions involving the pf shell. Due to a stronger tensor coupling effect $f(t)=3.1$, the shell gaps at $N=32,34$ are more closely with the experimental and theoretical results. This underscores that the tensor coupling effect plays a significant role in shaping relativistic symmetries and shell evolutions, particularly in exotic nuclei.

References

[1] O. Haxel, J. H. D. Jensen, and H. E. Suess, Phys. Rev. **75**, 1766 (1949)
[2] M. G. Mayer, Phys. Rev. **75**, 1969 (1949)
[3] A. Arima, M. Harvey, and K. Shimizu, Phys. Lett. B **30**, 517 (1969)
[4] K. T. Hecht and A. Adler, Nucl. Phys. A **137**, 129 (1969)
[5] J. N. Ginocchio, Phys. Rev. Lett. **78**, 436 (1997)
[6] J. Meng, K. Sugawara-Tanabe, S. Yamaji *et al.*, Phys. Rev. C **58**, R628 (1998)
[7] S.-G. Zhou, J. Meng, and P. Ring, Phys. Rev. Lett. **91**, 262501 (2003)
[8] H. Liang, J. Meng, and S.-G. Zhou, Phys. Rep. **570**, 1 (2015)
[9] J. Meng, K. Sugawara-Tanabe, S. Yamaji *et al.*, Phys. Rev. C **59**, 154 (1999)
[10] P. Alberto, R. Lisboa, M. Malheiro *et al.*, Phys. Rev. C **71**, 034313 (2005)
[11] Z. Ren, M. Mittig, B. Chen *et al.*, Phys. Rev. C **52**, R1764 (1995)
[12] W. H. Long, H. Sagawa, N. V. Giai *et al.*, Phys. Rev. C **76**, 034314 (2007)
[13] W. H. Long, T. Nakatsukasa, H. Sagawa *et al.*, Phys. Lett. B **680**, 428 (2009)
[14] W. H. Long, P. Ring, N. V. Giai *et al.*, Phys. Rev. C **81**, 024308 (2010)
[15] J. J. Li, W. H. Long, J. L. Song *et al.*, Phys. Rev. C **93**, 054312 (2016)
[16] A. Mutschler, A. Lemasson, O. Sorlin *et al.*, Nat. Phys. **13**, 152 (2017)
[17] W. H. Long, P. Ring, J. Meng *et al.*, Phys. Rev. C **81**, 031302(R) (2010)
[18] C. Delafosse, D. Verney, P. Marević *et al.*, Phys. Rev. Lett. **121**, 192502 (2018)
[19] W. S. Chen, D. P. Li, and J. Y. Guo, Sci. China-Phys. Mech. Astron. **59**, 682011 (2016)
[20] Z.-Z. Li, S.-Y. Chang, Q. Zhao *et al.*, Chin. Phys. C **43**, 074107 (2019)
[21] J. Geng, J. J. Li, W. H. Long *et al.*, Phys. Rev. C **100**, 051301(R) (2019)
[22] B. W, Q. Zhao, Z.-H. Wang *et al.*, Chin. Phys. C **44**, 074107 (2020)
[23] J. Geng, Y.-F. Niu, and W. H. Long, Chin. Phys. C **47**, 044102 (2023)
[24] J. Geng, P. W. Zhao, Y. F. Niu *et al.*, Phys. Lett. B **858**, 139036 (2024)
[25] Y. Peng, J. Liu, J. Geng *et al.*, Chin. Phys. C **49**, 064112 (2025)
[26] R. J. Furnstahl, J. J. Rusnak, and B. D. Serot, Nucl. Phys. A **632**, 607 (1998)
[27] G. Mao, Phys. Rev. C **67**, 044318 (2003)
[28] M. Chiapparini, A. O. Gattone, and B. K. Jennings, Nucl. Phys. A **529**, 589 (1991)
[29] R. Lisboa, M. Malheiro, A. S. de Castro *et al.*, Phys. Rev. C **69**, 024319 (2004)
[30] D.-P. Li, S.-W. Chen, and J.-Y. Guo, Phys. Rev. C **87**, 044311 (2013)
[31] J.-Y. Guo, S.-W. Chen, Z.-M. Niu *et al.*, Phys. Rev. Lett. **112**, 062502 (2014)
[32] D.-P. Li, S.-W. Chen, Z.-M. Niu *et al.*, Phys. Rev. C **91**, 024311 (2015)
[33] B. Huang, J.-Y. Guo, and S.-W. Chen, Phys. Rev. C **105**, 054313 (2022)
[34] B. Huang, J.-Y. Guo, Q. Liu *et al.*, Phys. Scr. **98**, 125304 (2023)
[35] Y. Guo and H. Liang, Phys Rev. C **99**, 054324 (2019)
[36] H. Liang, S. Shen, P. Zhao *et al.*, Phys. Rev. C **87**, 014334 (2013)
[37] S. Shen, H. Liang, P. Zhao *et al.*, Phys. Rev. C **88**, 024311 (2013)
[38] Q. Xu, Eur. Phys. J. A **51**, 81 (2015)
[39] X.-X. Shi, Q. Liu, and S.-W. Chen, Phys. Rev. C **113**, 024326 (2026)

[40] X.-X. Shi, B. Huang, and X.-N. Cao, Phys. Rev. C **111**, 034304 (2025)
[41] Y. Guo and H. Liang, Chin. Phys. C **43**, 114105 (2019)
[42] L. L. Foldy and S. A. Wouthuysen, Phys. Rev. **78**, 29 (1950)
[43] L. L. Foldy, Phys. Rev. **87**, 688 (1952)
[44] Z. X. Ren and P. W. Zhao, Phys. Rev. C **100**, 044322 (2019)
[45] Z. X. Ren and P. W. Zhao, Phys. Rev. C **102**, 021301 (2020)
[46] C. R. Ding, C. C. Wang, J. M. Yao *et al*., Phys. Rev. Lett. **136**, 052501 (2026)
[47] R.-Y. Zheng, X.-X. Sun, G.-F. Shen *et al*., Chin. Phys. C **48**, 014107 (2024)
[48] T. Lesinski, M. Bender, K. Bennaceur *et al*., Phys. Rev. C **76**, 014312 (2007)
[49] M. Moreno-Torres, M. Grasso, H. Liang *et al*., Phys. Rev. C **81**, 064327 (2010)
[50] L. Lalanne, O. Sorlin, A. Poves *et al*., Phys. Rev. Lett. **129**, 122501 (2022)
[51] L. Lalanne, O. Sorlin, A. Poves *et al*., Phys. Rev. Lett. **131**, 092501 (2023)
[52] S. Michimasa, M. Kobayashi, Y. Kiyokawa *et al*., Phys. Rev. Lett. **121**, 022506 (2018)
[53] F. Wienholtz, D. Beck, K. Blaum *et al*., Nature **498**, 346 (2013)
[54] D. Steppenbeck, S. Takeuchi, N. Aoi *et al*., Nature **502**, 207 (2013)
[55] S. Chen, J. Lee, P. Doornenbal *et al*., Phys. Rev. Lett. **123**, 142501 (2019)
[56] J. J. Li, J. Margueron, W. H. Long *et al*., Phys. Lett. B **753**, 97 (2016)
[57] L. Gaudefroy, A. Obertelli, S. Péru *et al*., Phys. Rev. C **80**, 064313 (2009)
[58] A. Magilligan, B. A. Brown, and S. R. Stroberg, Phys. Rev. C **104**, L051302 (2021)
[59] J. G. Li, B. S. Hu, Q. Wu *et al*., Phys. Rev. C **102**, 034302 (2020)
[60] S. Chen, F. Browne, P. Doornenbal *et al*., Phys. Lett. B **843**, 138025 (2023)
[61] E.-B Huo, K.-R. Li, X.-Y. Qu *et al*., Nucl. Sci. Tech. **34**, 105 (2023)
[62] D. Steppenbeck, S. Takeuchi, N. Aoi *et al*., Phys. Rev. Lett. **114**, 252501 (2015)
[63] H. N. Liu, A. Obertelli, P. Doornenbal *et al*., Phys. Rev. Lett. **122**, 072502 (2019)
[64] A. Huck, G. Klotz, A. Knipper *et al*., Phys. Rev. C **31**, 2226 (1985)
[65] D.-C. Dinca, R. V. F. Janssens, A. Gade *et al*., Phys. Rev. C **71**, 041302(R) (2005)
[66] M. Rosenbusch, P. Ascher, D. Atanasov *et al*., Phys. Rev. Lett. **114**, 202501 (2015)
[67] A. Gade, R. V. F. Janssens, D. Weisshaar *et al*., Phys. Rev. Lett. **112**, 112503 (2014)
[68] H. Hergert, S. K. Bogner, T. D. Morris *et al*., Phys. Rev. C **90**, 041302 (2014)
[69] G. Hagen, M. Hjorth-Jensen, G. R. Jansen *et al*., Phys. Rev. Lett. **109**, 032502 (2012)
[70] E. Yüksel, N. Van Giai, E. Khan *et al*., Phys. Rev. C **89**, 064322 (2014)
[71] M. Grasso, Phys. Rev. C **89**, 034316 (2014)
[72] D. Vretenar, A. V. Afanasjev, G. A. Lalazissis *et al*., Phys. Rep. **409**, 101 (2005)
[73] P. Ring, Prog. Part. Nucl. Phys. **37**, 193 (1996)
[74] J. Meng, H. Toki, S. G. Zhou *et al*., Prog. Part. Nucl. Phys. **57**, 470 (2006)
[75] T. Nikšić, D. Vretenar, and P. Ring, Prog. Part. Nucl. Phys. **66**, 519 (2011)
[76] C. Bahri, J. P. Draayer, and S. A. Moszkowski, Phys. Rev. Lett. **68**, 2133 (1992)
[77] J. Liu, Y. F. Niu, and W. H. Long, Phys. Lett. B **806**, 135524 (2020)
[78] F. Wegner, Ann. Physik **506**, 77 (1994)
[79] J.-Y. Guo, Phys. Rev. C **85**, 021302 (2012)
[80] R. Lisboa, M. Malheiro, P. Alberto *et al*., Phys. Rev. C **81**, 064324 (2010)
[81] A. Klose, K. Minamisono, A. J. Miller *et al*., Phys. Rev. C **99**, 061301(R) (2019)
[82] C. D. Kavaloski, G. Bassani, and N. M. Hintz, Phys. Rev. **132**, 813 (1963)
[83] J. H. E. Mattauch, W. Thiele, and A. H. Wapstra, Nucl. Phys. **67**, 32 (1965)
[84] L. R. B. Elton and A. Swift, Nucl. Phys. A **94**, 52 (1967)
[85] X. Campi and D. W. Sprung, Nucl. Phys. A **194**, 401 (1972)
[86] N. Schwierz, I. Wiedenhover, and A. Volya, arXiv: 0709.3525.
[87] H. Nakada and T. Inakura, Phys. Rev. C **110**, L051301 (2024)
[88] T. W. Conlon, B. F. Bayman, and E. Kashy, Phys. Rev. **144**, 941 (1966)
[89] E. Kashy, A. Sperduto, H. A. Enge *et al*., Phys. Rev. **135**, B865 (1964)
[90] T. A. Belote, A. Sperduto, and W. W. Buechner, Phys. Rev. **139**, B80 (1965)
[91] A. Gade, R. V. F. Janssens, D. Bazin *et al*., Phys. Rev. C **74**, 021302 (2006)
[92] T. R. Rodríguez and J. Luis Egido, Phys. Rev. Lett. **99**, 062501 (2007)
[93] M. Baldo, P. F. Bortignon, G. Colò *et al*., J. Phys. G: Nucl. Part. Phys. **42**, 085109 (2015)
[94] T. Duguet, H. Hergert, J. D. Holt *et al*., Phys. Rev. C **92**, 034313 (2015)
[95] E. V. Litvinova and A. V. Afanasjev, Phys. Rev. C **84**, 014305 (2011)